presence of ammonia remain subject to oxygen regulation[11]. It is also unlikely that the products of the *nifHDK* operon are involved in oxygen repression because the level of β-galactosidase activity in a haploid polar *nifH::lac* fusion strain was lower under a D.O.T. of 0.5% than the control under nitrogen. It is possible that one of the other products of the *nif* gene cluster acts as an oxygen sensor and can mediate oxygen repression at a low D.O.T., whereas at higher oxygen concentrations there is a more general effect on the *nif* gene cluster which may also extend to other oxygen-repressible systems in the cell.

The isolation of regulatory mutations in each of the *nif* transcriptional units should considerably enhance our knowledge of the regulation of this complex gene cluster.

We thank Dawn Allitt, Marie Clark, Simon Harrison and Eugene Kavanagh for technical assistance, John Postgate for constructive criticism of the manuscript, and Malcolm Casadaban for supplying unpublished information and useful strains. M.I. and D.K. were supported by EMBO fellowships.

Received 4 March; accepted 23 April 1980.

1. Eady, R. R. & Smith, B. E. in *A Treatise on Dinitrogen Fixation*, Sections I, II (eds Hardy, R. W., Bottomly, F. & Burns, R. C.) 399–490 (Wiley, New York, 1979).
2. Shah, V. K. & Brill, W. J. *Proc. natn. Acad. Sci. U.S.A.* **74,** 3249–3253 (1977).
3. Eady, R. R. & Postgate, J. R. *Nature* **249,** 805–810 (1974).
4. Merrick, M., Filser, M., Kennedy, C. & Dixon, R. *Molec. gen. Genet.* **165,** 103–111 (1978).
5. Elmerich, C., Houmard, J., Sibold, L., Manheimer, I. & Charpin, N. *Molec. gen. Genet.* **165,** 181–189 (1978).
6. MacNeil, T., MacNeil, D., Roberts, G. P., Supiano, M. A. & Brill, W. J. *J. Bact.* **136,** 253–266 (1978).
7. Merrick, M. *et al. J. gen. Microbiol.* **117,** 509–520 (1980).
8. Roberts, G. P., MacNeil, T., MacNeil, D. & Brill, W. J. *J. Bact.* **136,** 267–279 (1978).
9. Hill, S. & Kavanagh, E. *J. Bact.* **141,** 470–475 (1980).
10. Dixon, R., Kennedy, C., Kondorosi, A., Krishnapillai, V. & Merrick, M. *Mol. gen. Genet.* **157,** 189–198 (1977).
11. Eady, R. R., Issack, R., Kennedy, C., Postgate, J. R. & Ratcliffe, H. D. *J. gen. Microbiol.* **104,** 277–285 (1978).
12. Brill, W. J., Steiner, A. L. & Shah, V. K. *J. Bact.* **118,** 986–989 (1974).
13. Tyler, B. *A. Rev. Biochem.* **47,** 1127–1162 (1978).
14. Casadaban, M. & Cohen, S. N. *Proc. natn. Acad. Sci. U.S.A.* **76,** 4530–4533 (1979).
15. Janssen, K. A., Riedel, G. E., Ausubel, F. M. & Cannon, F. C. in *Proc. 3rd int. Symp. Nitrogen Fixation*, Vol. 1 (eds Orme-Johnson, W. H. & Newton, W.) 85–93 (University Park Press, Baltimore, 1980).
16. Pahel, G. & Tyler, B. *Proc. natn. Acad. Sci.* U.S.A. **76,** 4544–4548 (1979).
17. Kustu, S., Burton, D., Garcia, E., McCarter, L. & McFarland, N. *Proc. natn. Acad. Sci. U.S.A.* **76,** 4576–4580 (1979).
18. Ausubel, F. M., Reidel, G., Cannon, F., Peskin, A. & Margolskee, R. in *Genetic Engineering for Nitrogen Fixation* (ed. Hollaender, A.) 111–126 (Plenum, New York, 1977).
19. Kennedy, C. & Postgate, J. R. *J. gen. Microbiol.* **98,** 551–557 (1977).
20. Cannon, F. C., Dixon, R. A., Postgate, J. R. & Primrose, S. B. *J. gen. Microbiol.* **80,** 227–239 (1974).
21. Kelly, M. & Lang, G. *Biochim. biophys. Acta* **223,** 86–104 (1970).
22. Miller, J. H. in *Experiments in Molecular Genetics*, 162–172 (Cold Spring Harbor Laboratory, New York, 1972).

# LETTERS

## IUE observations of the UV spectrum of comet Bradfield

**P. D. Feldman*, H. A. Weaver*, M. C. Festou†, M. F. A'Hearn‡, W. M. Jackson§, B. Donn, J. Rahe||¶, A. M. Smith|| & P. Benvenuti||#**

*Johns Hopkins University, Baltimore, Maryland 21218
†University of Michigan, Ann Arbor, Michigan 48109
‡University of Maryland, College Park, Maryland 20742
§Howard University, Washington, DC 20059
||Goddard Space Flight Center, Greenbelt, Maryland 20771
#ESA-VILSPA, Madrid, Spain

**Comet Bradfield (1979l), discovered shortly after perihelion, on Christmas day 1979, is characterized by a retrograde orbit of period ≈250 yr. This orbit was very favourable for observation by the IUE satellite[1], and the first observations, the preliminary results of which are reported here, were made on 10 and 11 January 1980. Previously, comprehensive vacuum UV cometary spectra were available only for Comet West (1976VI) from rocket observations[2,3] and Comet Seargent (1978m) obtained with IUE[4], hence three comets have now been observed in the wavelength region where most of the major constituents are detectable spectroscopically. The UV spectra of these comets are remarkably similar, despite large differences between them in the gas-to-dust ratio and the different heliocentric distances at which the observations were made, and although the statistical basis is still very small, the implication for cosmogony is that nearly all comets have the same primary composition and origin.**

At the time of these observations the comet was 0.71 AU from the Sun, 0.61 AU from Earth, and had a total visual magnitude ≈4. The visual appearance of the comet was diffuse with a weak central condensation and with only a slight trace of an ion tail. The comet could be tracked on its centre of brightness by the fine error sensor of the IUE. Drift was found to be no more than 1–2 arc s $h^{-1}$. All observations were made with the large (10 × 20 arc s) apertures of the spectrographs and the pointing accuracy was verified by the presence of the weak continuum near 2,900 Å in the centre of the slit.

The short wavelength spectrum is shown in a 2-h exposure in Fig. 1. The vertical scale has been reduced to average surface brightness per Å in the 10 × 20 arc s slit. As noted below, the use of the large slit permits a limited amount of spatial imaging on extended sources[5] to a resolution of ≈6 arc s, but the spectra presented here represent the average over the entire slit. The dominant features in the spectrum other than H I Lyα which is highly over-exposed are O I λ1,302, C I λλ1,561, 1,657 and 1,931 and S I λ1,813, as in the spectrum of Comet West[2,3]. The brightness in a given line or multiplet is obtained by integrating over the instrumental spectral band-pass which varies from ≈6 Å for a point source to ≈11 Å for a diffuse source uniformly filling the entire aperture. Table 1 gives the average brightness for these features. The C II λ1,335 multiplet and CO fourth positive bands observed by Feldman and Brune[2], are present in the smoothed spectrum of Fig. 1 slightly above the noise at about the same level relative to the C I lines as in the spectrum of Comet West. It is surprising that the spectrum of Comet

**Table 1** Average brightness of spectral features at 0.71 AU

| Species | Wavelength (Å) | Brightness (kR) |
|---|---|---|
| H I Lyα | 1,216 | 160 |
| O I | 1,304 | 0.33 |
| C I | 1,561 | 0.12 |
| | 1,657 | 0.55 |
| | 1,931 | 0.05 |
| S I | 1,807–1,826 | 0.26 |
| CS (0,0) | 2,576 | 1.40 |
| (0,1) | 2,663 | 0.15 |
| $CO_2^+$ | 2,890 | 0.60 |
| OH (1,0) | 2,820 | 7.6 |
| (0,0) | 3,085 | 370 |
| (1,1) | 3,142 | 12 |
| $CO^+$ (0,1)+(1,2) | 2,321 | 0.39 |
| (0,2)+(1,3) | 2,436 | 0.18 |

†Permanent address: Service d'Aéronomie du CNRS, Verrières-le-Buisson, France; ¶Permanent address: Astronomical Institute, Universität Erlangen, Nürnberg, FRG.

0028-0836/80/280132-04$01.00

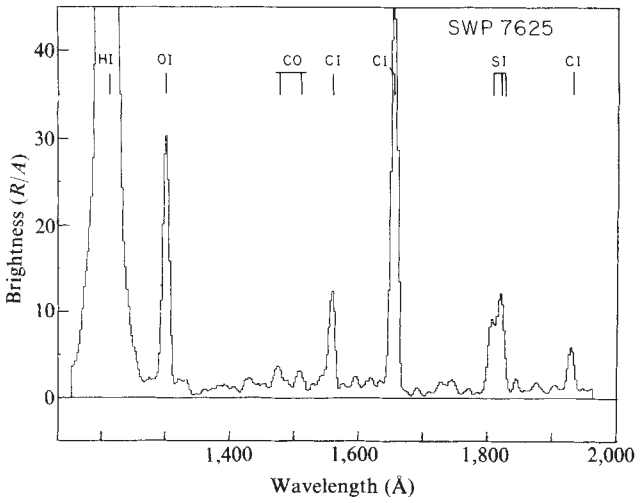


**Fig. 1** Low dispersion, short wavelength spectrum of Comet Bradfield taken with the IUE spectrograph slit centred on the visible centre of brightness on 10 January 1980. The exposure time was 2 h.

Bradfield is so similar to that of Comet West considering the differences in appearance, heliocentric distance and gas production rate at the times of observation as well as the difference in projected slit area of the two instruments. This suggests that reactions among the neutral and ionized species in the inner coma may not play a significant part in altering the composition of the coma following photodestruction of the mother molecules evaporated from the cometary nucleus.

The average brightness of the H I Ly$\alpha$ emission, which is saturated in the spectrum of Fig. 1, is determined from a 60-s exposure and is found to be 160 kR which indicates an optically thick atomic hydrogen column along the line-of-sight to the centre of the coma. The O I multiplet at 1,302 A is nearly optically thick as it is excited by resonance scattering of the solar $\lambda$1,302 lines because the heliocentric velocity of the comet was 24 km s$^{-1}$. In previous observations of Comets Kohoutek and West[2] this velocity was $\approx$50 km s$^{-1}$ which shifted the cometary oxygen absorption outside the solar line profile and it was assumed that fluorescent pumping by solar H I Ly$\beta$ radiation was the excitation source[6].

A 2-h exposure of the long wavelength spectrum is shown in Fig. 2. Once again the dominant features are the $CO^+$, CS, $CO_2^+$, and OH bands identified previously[3], but now the identification of CS is confirmed by the presence of the (0,1) band at 2,663 Å and the (1,0) band at 2,507 Å in addition to the saturated (0,0) band at 2,576 Å, all three of which are

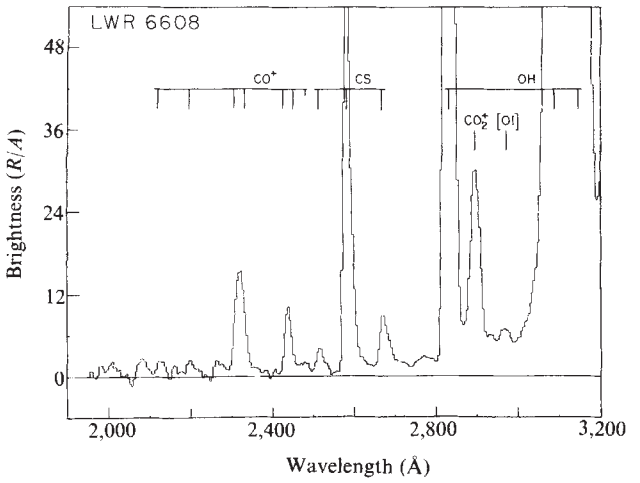


**Fig. 2** Same as Fig. 1, but a 2-h exposure with the long wavelength spectrograph.

degraded towards the red. The three OH bands are also saturated but the average brightness of these bands can be found from shorter exposures. These are all listed in Table 1. The weak continuum observed near 2,750 and 2,950 Å suggests a very small dust-to-gas ratio for this comet, consistent with visual observations.

One peculiarity of this spectrum is the absence (or extreme weakness) of the (0,0) and (1,0) bands of the $CO^+$ first negative system near 2,190 and 2,112 Å, respectively. Both of these bands are also absent or very weak in the IUE spectrum of Comet Seargent[4]. In the rocket spectra of Comet West[2,3] the (0,0) band was the strongest $CO^+$ feature. It does not seem likely that fluorescent pumping by solar radiation can explain this difference as the observed strong bands near 2,300 (0,1 and 1,2) and 2,420 Å (0,2 and 1,3) originate on the same $v'=0$ and 1 levels of the upper $B^2\Sigma^+$ state of $CO^+$ and in an optically thin ion coma the band intensities would be proportional to the Franck–Condon factors for the transitions. One possibility is that the $CO^+$ in our field of view is optically thick along the line-of-sight in the $v''=0$ ground state and as a result (0,0) and (1,0) band photons are re-absorbed and pumped into transitions such as (0,1) and (1,2). The difference with the Comet West data can be explained by the difference in field of view, $5\times35$ arc min for the experiment of Feldman and Brune[2] compared with $10\times20$ arc s for IUE, a factor of $\approx$3,200 in solid angle. Thus, most of the radiation observed by Feldman and Brune is from $CO^+$ significantly further away from the nucleus where the $CO^+$ is not optically thick along the line-of-sight, and the relative band intensities are close to the theoretically expected values. A consequence of this explanation is the inference that $CO^+$ is produced in large abundance within 3,000 km of the nucleus. However, this hypothesis is not consistent with visual spectra obtained later in the month (January 30.0) which showed only very weak emission in the $CO^+$ comet tail bands near 4,000 Å (C. McCracken, personal communication) and only a faint visual ion tail.

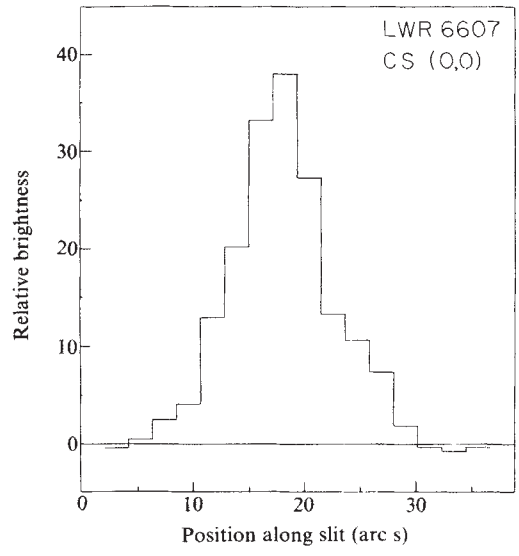


**Fig. 3** Variation of the brightness of the CS (0,0) band at 2,576 Å across the spectrograph slit. At the instrumental resolution of 6 arc s, the CS seems to have a point-source origin.

Several very weak features were observed in both Fig. 1 and Fig. 2 and may, in fact, be real emission features such as additional CO fourth positive bands or the [O I] line at 2,972 Å. There is strong evidence that the [O I] 2,972 Å feature is real as it is also present above the dust continuum in the spectra of Comet West[2,3]. This transition ($^1S$–$^3P$), known to atmospheric spectroscopists as the 'trans-auroral' line of

oxygen, is produced at 5% of the rate of the 'auroral green line' at 5,577 Å ($^1S$–$^1D$). The green line has been proposed[7] but not conclusively identified in cometary spectra due to the masking effect of the solar scattered continuum, the nearby (1,2) Swan band of $C_2$ and the presence of this line in the night airglow, but it is clear that oxygen in the $^1S$ state is produced in the coma. Preliminary calculations indicate that direct photodissociation of $H_2O$ by solar H I Lyα radiation is sufficient to account for the observed surface brightness of the λ2,972 Å feature.

The spatial variations of the UV emissions can be studied in two ways. For those emissions with short scale lengths there is an appreciable variation in brightness within the 10 × 20 arc s aperture of the spectrographs and the variation can be mapped with a spatial resolution of ≈6 arc s. Otherwise it is necessary to take several different exposures with the spectrograph slit offset by a known amount from the centre of visual brightness of the coma. An example of the former is the CS (0,0) band at 2,576 Å, for which the spatial variation in the large slit from a 30-min exposure is shown in Fig. 3. The horizontal scale is the linear distance from the centre of the coma appropriate to the Earth–comet distance at the time of observation. The sharp decrease in brightness away from the centre of the comet suggests a $\rho^{-1}$ brightness dependence characteristic of a parent molecule density distribution which varies as $R^{-2}$ close to the nucleus, where $R$ is the distance from the centre of the comet and $\rho$ is the distance from the centre projected onto the sky. It is thus very probable that CS exists as a parent molecule in the cometary ice or is the dissociation product of an extremely short-lived parent molecule.

The second technique, several exposures centred at different distances from the visible centre of brightness, is shown for the OH (0,0) band at 3,090 A in Fig. 4. The three data points are compared with the predictions of a Haser model[8] to give both the scale length (at 1 AU) and the OH production rate. However, the results are sensitive to the choice of the assumed $H_2O$ outflow velocity and for our purpose we took extreme cases of 0.5 and 1.0 km s$^{-1}$. The other parameters needed[9] are the $H_2O$ lifetime, $8.2 \times 10^4$ s, and the OH outflow velocity, 1.15 km s$^{-1}$. The two curves in Fig. 4, virtually indistinguishable from each other, correspond to values of $\tau_{OH} = 1.0 \times 10^5$ s and $5.0 \times 10^4$ s for the respective values of $v_{H_2O} = 0.5$ and 1.0 km s$^{-1}$. The corresponding values of the OH (and presumably $H_2O$) production rate at 0.71 AU are $Q_{OH} = 1 \times 10^{29}$ s$^{-1}$ and $2 \times 10^{29}$ s$^{-1}$, respectively. The range of deduced values of $\tau_{OH}$ (at 1 AU) is in accord with the theoretical value

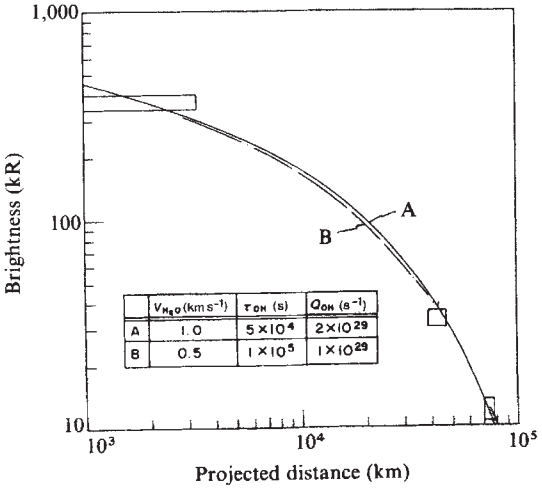


**Fig. 4** Comparison of the OH (0,0) band brightness profile with a radial outflow model using the parameters defined in the insert. Data from three exposures are shown as rectangular boxes, the horizontal size being the projected length of the spectrograph slit on the comet and the vertical size the measurement uncertainty.

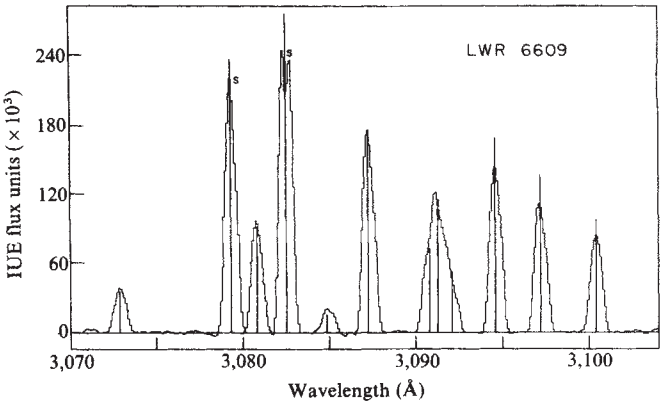


**Fig. 5** High dispersion spectrum of the OH (0,0) band taken from a 15-min exposure. The wavelengths shown are vacuum wavelengths. The ordinate is in IUE flux units which are not corrected for the absolute spectral response of the instrument. The theoretical intensities have been multiplied by the approximate spectral response curve of the long-wavelength camera which varies steeply in this spectral region. The $P_1(1)$ line near 3,082 Å was saturated (S) in the observed spectrum and is off-scale in the theoretical calculation.

of $7.5 \times 10^4$ s given by Jackson[10] for a heliocentric velocity of 24 km s$^{-1}$. According to Festou[9], the lifetime derived by means of Haser's model is a lower limit to that obtained from a model which properly accounts for the spatial distribution of the OH radicals produced by photodissociation. The water production rate, reduced to 1 AU, of $0.5$–$1 \times 10^{29}$ s$^{-1}$, is considerably lower than that of several 'new' comets as given by Keller and Lillie[11], consistent with the identification of this comet as a long-period comet which has made numerous passes through the inner Solar System.

Assuming that CS is evaporated from the nucleus with the same outflow velocity as $H_2O$, it is possible to determine the relative production rate of these two molecules. A g-factor for the CS (0,0) band at 2,576 Å of $7 \times 10^{-4}$ photons per s per molecule at 1 AU was adopted which leads to a value of the ratio $Q_{CS}/Q_{H_2O} \approx 5 \times 10^{-4}$. Thus, although CS is a prominent feature of the UV cometary spectrum it is clearly only a minor species in the comet.

The high resolution capability of the IUE spectrographs was used to study further the resonance fluorescence excitation of the OH (0,0) band, the strongest emission feature in the cometary spectrum. A 15-min, high-dispersion exposure is shown in Fig. 5, along with the predicted relative intensities as calculated for the heliocentric distance, $r$, and radial velocity, $\dot{r}$, at the time of observation[12]. The excellent agreement between theory and observation over the velocity range 24–28 km s$^{-1}$ indicates that no process other than fluorescence is important in controlling the OH level populations. The dependence of the spectrum on $\dot{r}$ is strikingly illustrated by comparison of Fig. 5 with a similar, high-dispersion spectrum of this band from Comet Seargent (1,978m) (ref. 4), which differed in heliocentric radial velocity by ~10 km s$^{-1}$. The large changes in the spectrum with radial velocity indicate that the fluorescence efficiency (g-factor) is also a function of radial velocity. The velocity dependent g-factors, needed to convert low resolution fluxes to column densities as above, were obtained from this high resolution analysis.

These new results are only the preliminary analysis of the data obtained at the first opportunity for IUE observations of Comet Bradfield. Observations were continued, at the rate of one a week corresponding to increments in heliocentric distance of ~0.1 AU, through February, and should provide important information about the variation of the production rates of the UV active species with distance from the Sun. As the first comet to be so regularly observed in the vacuum UV, Comet Bradfield will greatly increase our understanding of the physics and chemistry of the cometary atmosphere.

We thank the IUE Observatory staff for acquisition and reduction of the data and for all their assistance. B. G. Marsden and M. P. Candy provided up-to-the-minute ephemerides. The work at Johns Hopkins University is supported by NASA grant NSG 5393.

*Note added in proof:* Further analysis has disclosed that the features at 2,321 and 2,436 Å are incorrectly identified as $CO^+$; rather they are a Mulliken band of $C_2$ and the second order HILyα image, respectively. The absence of $CO^+$ bands in the UV is thus consistent with the absence of this species in the visible spectrum.

Received 17 March; accepted 23 April 1980.

1. Boggess, A. *et al. Nature* **275**, 377–385 (1978).
2. Feldman, P. D. & Brune, W. H. *Astrophys. J. Lett.* **209**, L45–L48 (1976).
3. Smith, A. M. & Casswell, L. *Astrophys. J.* (submitted).
4. Jackson, W. M. *et al. Astr. Astrophys.* **73**, L7–L9 (1978).
5. Clarke, J. T., Moos, H. W., Atreya, S. K. & Lane, A. L. *Science* (submitted).
6. Feldman, P. D., Opal, C. B., Meier, R. R. & Nicolas, K. R. in *The Study of Comets* (eds Donn, B. *et al.*) 773–795 (NASA SP-393, 1976).
7. Swings, P. *Q. Jl R. astr. Soc.* **6**, 28–69 (1965).
8. Haser, L. *Bull. Acad. r. Belg.* **43**, 740–750 (1957).
9. Festou, M. thesis, Univ. Paris VI (1978).
10. Jackson, W. M. *Icarus* **41**, 147–152 (1980).
11. Keller, H. U. & Lillie, C. F. *Astr. Astrophys.* **62**, 143–147 (1978).
12. Schleicher, D. & A'Hearn, M. F. (in preparation).
13. Despois, D., Gerard, E., Crovisier, J. & Kazès, I. *Trans. IAU* (in the press).

# Tidal effects on the mass profile of galactic haloes

**Avishai Dekel*, Myron Lecar† & Jacob Shaham***

*Racah Institute of Physics, The Hebrew University of Jerusalem, Jerusalem, Israel
†Harvard-Smithsonian Center for Astrophysics, Cambridge, Massachusetts 02138

**Most spiral galaxies are believed to be embedded in dark massive haloes[1,2]. The main observational evidence for their presence is the rotation curves of edge-on disks at large radii measured both by optical[3,23] and radio (21 cm)[4] techniques: rotation velocities remain constant to distances of several tens of kiloparsecs, far beyond the main visible bodies of the galaxies. This suggests the existence of a dark halo whose mass, if spherical, varies linearly with distance $R$ from the galactic centre and hence has a density profile which falls off as $R^{-2}$. The extended 'flat' shape of the haloes poses a problem for most theoretical hypotheses of galaxy formation because simulations of collapse[5–8] and of violent mergers[9] predict a spherical density profile which is rather Hubble-like ($\rho \propto R^{-3}$) or even steeper. The time scale for two-body relaxation, which can lead to a flatter, isothermal, density profile, is much larger than the Hubble time. If, as Gunn[10] and Gott[6] have suggested, secondary cosmological infall produces the $\rho \propto R^{-2}$ haloes, special initial conditions are required: (1) the central perturbation, which is the progenitor of the galaxy, needs to be initially embedded in a bound homogeneous background—an assumption which might not be fully justified for relatively isolated galaxies; and, (2) the infall must be such that there is no dissipation so that most of the mass should already be in the form of compact objects before halo formation. We suggest, as an alternative mechanism, tidal interactions between haloes, or possibly between their smaller building blocks, while in the hierarchical gravitational clustering process. In this process typical tidal encounters are slow, such that relative orbital velocities of the interacting systems are comparable to the internal velocities of the stars in each system. The two systems are slightly unbound.**

Our suggestion is based on $N$-body simulations which we performed to study the tidal effects of such encounters on the mass-profile of spherical systems[11]. On adopting the common view, that the dark material is not gaseous[12–14] but is rather composed of condensed bodies (such as unevolved low-mass stars, dead remnants of old stars, and primordial black holes[15]), a dissipationless $N$-body system was assumed to represent properly a galactic halo. The numerical experiments

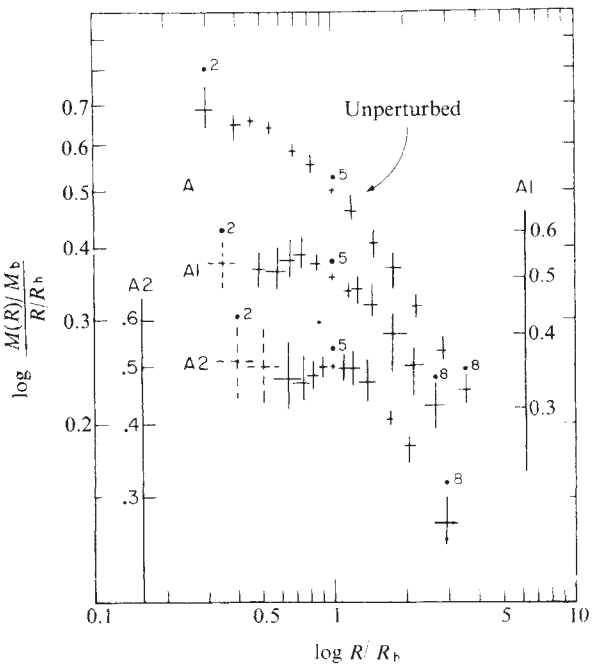


**Fig. 1** Rotation curves of two tidally perturbed haloes, A1 and A2, are compared with the unperturbed one at the same final time. The mass and the radius are in fractional units relative to the mass, $M_h$, and the half-mass-radius, $R_h$, of the remnant bound system. The symbols correspond to given fractions of the bound mass, separated by 5%, and the error bars correspond to temporal deviations over three successive crossing-times. The curves are vertically shifted by a factor of 1/2 relative to each other. The parameters for the cases A1 and A2 are the following, perturber mass/halo mass = 2; relative velocity at closest approach = 1.05 the parabolic velocity; closest approach distance = 4.6 $R_h$, 2.8 $R_h$; fractional mass loss = 0.22, 0.33; final $R_h$/original $R_h$ = 0.8, 0.74. Note that both the fractional and absolute flat regions become more extended.

were based on the $N$-body code developed by Aarseth[7,16,17]. It integrates the equations of motion of $N$ softened particles, which interact through a potential

$$\phi_{ij} = -Gm_i m_j/[(r_i - r_j)^2 + \varepsilon^2]^{\frac{1}{2}}. \quad (1)$$

The softening parameter, $\varepsilon$, is chosen to suppress the two-body relaxation effects that arise due to the small number of particles in our experiment.

In our experiments, a 250-body system was tidally perturbed by a point perturber of comparable mass. The encounter velocities were slightly above parabolic and the closest approach distances, $p$, were between 2.5 $R_h$ and 5 $R_h$, where $R_h$ was the half-mass-radius. In such conditions, each 'shell' of stars expands, gradual stripping occurs outside $\sim R_h$ and up to one-third of the original mass may become unbound. As Fig. 1 shows, the effect on a system which initially has a decreasing $M(R)/R$ profile ($\rho \propto R^{-3}$) is to steepen the profile in the outer parts, and to produce, or extend, an inner region of constant $M(R)/R$, to encompass 50–70% of the bound mass. Hence, this mechanism, whose exact relaxation nature is not yet understood theoretically, produces systems which might show flat rotation curves over a large fraction of their mass (but not a relaxed flat outer envelope, as was discussed previously[18,19]). Tandem encounters of the same system tend to strip the outer parts and produce a smaller system, which retains a flat inner profile.

Most of the stripped stars in our simulations did not become bound to the perturber but rather escaped from the two-body system altogether. This indicates that stripped material from a realistic, $N$-body, perturber would not become bound to the perturbed system and, therefore, have no substantial effect on its mass profile. We therefore assume that

0028-0836/80/280135-02$01.00